ADVANCING EARTH AND SPACE SCIENCES

Geophysical Research Letters

RESEARCH LETTER
10.1029/2026GL122478

M. Tesche and H. Andersen contributed equally to this work.

Key Points:

- CALIOP reveals anti-correlated low-cloud cover and top-height trends, suggesting a joint response to changes in controlling factors
- Low-cloud cover and cloud top height show opposite responses to higher sea-surface temperature (SST) and stronger inversions
- Stratocumulus regions show the strongest change in low-cloud cover and top height consistent with the stratocumulus-to-cumulus transition

Supporting Information:

Supporting Information may be found in the online version of this article.

Correspondence to:

M. Tesche,
matthias.tesche@uni-leipzig.de

Citation:

Tesche, M., Andersen, H., Choudhury, G., & Goren, T. (2026). Trends and sensitivities of low-cloud cover and top height from spaceborne lidar observations. *Geophysical Research Letters*, *53*, e2026GL122478. https://doi.org/10.1029/2026GL122478

Received 23 FEB 2026
Accepted 1 JUL 2026

Author Contributions:

Conceptualization: M. Tesche, H. Andersen, G. Choudhury, T. Goren
Formal analysis: M. Tesche, H. Andersen
Investigation: M. Tesche, H. Andersen
Methodology: M. Tesche, H. Andersen, G. Choudhury, T. Goren
Software: H. Andersen
Visualization: M. Tesche, H. Andersen
Writing – original draft: M. Tesche, H. Andersen, G. Choudhury, T. Goren
Writing – review & editing: M. Tesche, H. Andersen, G. Choudhury, T. Goren

Trends and Sensitivities of Low-Cloud Cover and Top Height From Spaceborne Lidar Observations

M. Tesche[1], H. Andersen[2,3], G. Choudhury[4], and T. Goren[4]

[1]Leipzig Institute for Meteorology, Leipzig University, Leipzig, Germany, [2]Karlsruhe Institute of Technology (KIT), Institute of Meteorology and Climate Research Atmospheric Trace Gases and Remote Sensing, Karlsruhe, Germany, [3]Karlsruhe Institute of Technology (KIT), Institute of Photogrammetry and Remote Sensing, Karlsruhe, Germany, [4]Department of Geography and the Environment, Bar-Ilan University, Tel Aviv, Israel

Abstract Low clouds effectively cool the Earth by reflecting incoming solar radiation. Detecting low-level clouds with passive satellite sensors can be ambiguous, whereas active remote sensing instruments directly measure cloud-top height. Here, we analyze 14 years of spaceborne lidar observations to assess trends in the occurrence of low-level clouds and their cloud-top height. We find that spatial trend patterns in low-level cloud cover and low-level cloud top height are negatively correlated, that is, regions with a decrease in low-cloud cover tend to show an increase in cloud-top height. We find that spatial trend patterns can be well explained by sea-surface temperature (SST) and estimated inversion strength. Low-level clouds in climatological stratocumulus regions are particularly sensitive to changes in SST (-3.4 to $-3.7\,\%\,K^{-1}$ in cloud cover and $50\,m\,K^{-1}$ in cloud-top height) and estimated inversion strength ($3.3\,\%\,K^{-1}$ in cloud cover and $-69\,m\,K^{-1}$ in cloud-top height).

Plain Language Summary Low-level clouds play an important role in the Earth's energy budget because of their capability to reflect large amounts of incoming sunlight. However, the detection of low-level clouds in satellite observations is not always straightforward. Only active remote sensing with spaceborne lidar or radar can provide direct measurements of cloud-top height and thus lead to the unambiguous detection of low-level clouds. Here, we have analyzed 14 years of spaceborne lidar observations for trends in the occurrence of low-level clouds and their cloud-top height. We find that spatial trend patterns in low-level cloud cover and low-level cloud top height are negatively correlated, that is, regions with a decrease in cloud cover tend to show an increase in cloud-top height. We find that spatial trend patterns can be well explained by SST and estimated inversion strength. These parameters are particularly important for the occurrence and top height of low-level clouds in climatological stratocumulus regions.

1. Introduction

Low clouds play an important role in the Earth's energy budget by modulating planetary albedo. They have a strong cooling effect as they reflect large amounts of incoming solar radiation and prevent the absorption of energy by the Earth's surface. Even small changes in the spatial extent or brightness of low clouds can therefore produce a radiative effect on the order of that related to a doubled concentration of carbon dioxide in the atmosphere (Slingo, 1990).

In recent years, observations have revealed a gradual decrease in planetary albedo (Goode et al., 2021) that contributes to the increase in Earth's energy imbalance (Mauritsen et al., 2025). The albedo decrease and the resulting global temperature increase have been attributed to a decrease in low-level cloud cover (LCC), particularly over the northern hemispheric oceans, the south Atlantic, and continental regions with deep convection (Ceppi et al., 2026; Goessling et al., 2025; Loeb et al., 2018; Zelinka et al., 2026). The most abundant type of low cloud is stratocumulus, which is prevalent over the subtropical eastern oceans under conditions of strong lower-tropospheric stability, subsidence in the free troposphere, and an ample supply of surface moisture (Klein & Hartmann, 1993; Wood, 2012). Over the ocean, increased sea-surface temperature (SST) can lead to a positive feedback, that is, further SST increase due to a decrease in LCC (Eastman et al., 2011). But LCC also depends on the structure of the marine boundary layer, entrainment at cloud top, larger-scale meteorological conditions in the free troposphere, changes in aerosol concentration, and cloud feedbacks (Andersen et al., 2017; Christensen et al., 2020; Goren et al., 2022; Jia et al., 2024; Klein & Hartmann, 1993; Myers et al., 2021; Naud et al., 2023; Scott et al., 2020; Wood, 2012). Studies that consider a variety of cloud-controlling factors generally conclude that SST and estimated inversion strength (EIS) are among the most influential for LCC (Andersen et al., 2022; Cao et al., 2024; Ceppi et al., 2026; McCoy et al., 2017; Qu et al., 2015; Scott et al., 2020).

Trends in LCC have been shown to be associated with changes in cloud vertical structure (Cesana et al., 2019; Liu et al., 2024), which can in turn affect both longwave and shortwave radiative effects (Choudhury & Goren, 2024; Denby, 2020). However, most studies investigating trends in LCC rely on observations from passive sensors (Ceppi et al., 2026; Geiss & Marchand, 2019; Marchand, 2013; Zelinka et al., 2026), which tend to underestimate cloud-top height, particularly for thin clouds (Huo et al., 2020; Mitra et al., 2021), and are therefore not well suited to detecting changes in cloud-top height. Cesana et al. (2019) and Liu et al. (2024) use observations from the Cloud-Aerosol Lidar with Orthogonal Polarization (CALIOP) lidar aboard the Cloud-Aerosol Lidar and Infrared Pathfinder Satellite Observations (CALIPSO) satellite (Winker et al., 2009) to assess changes in cloud vertical structure in response to changes in surface temperature and lower-tropospheric stability. They find that increasing SST and decreasing EIS lead to a decrease in LCC and an increase in cloud-top height for marine stratocumulus. However, a comprehensive quantification of the sensitivity of low-cloud top height (Z_{top}) to changes in SST or EIS (or lower-tropospheric stability) is still lacking. In another demonstration of the potential for deriving long-term trends from CALIOP measurements, Chepfer et al. (2025) find a decrease in cloud cover and a rise in cloud altitude for opaque clouds based on nighttime data.

Global climate models (GCMs) generally predict a decrease in LCC and an increase in Z_{top} in a warmer climate (e.g., Forster et al., 2021). The accurate description and prediction of how the properties of low-level clouds might change in a warming world are essential for reliable climate predictions. The relationship between albedo, LCC, and SST is found to be an important factor in the latest generation of GCMs (Zelinka et al., 2020). Comparisons between observations and GCM simulations can be used to constrain model representations of low-cloud–related albedo changes and to identify models that are more likely to reliably simulate future behavior (Cesana et al., 2019; McCoy et al., 2017; Myers & Norris, 2016).

Here, we use a 14-year CALIOP data set to identify the presence of low-level clouds and their Z_{top}, and whether or not those co-occur with clouds higher up. The resulting data set is used to investigate trends in LCC and Z_{top} and to quantify their sensitivity to changes in SST and EIS. We focus specifically on unobscured low clouds to account for variation in higher level clouds, and because changes in their occurrence have a strong and direct impact on planetary albedo. Section 2 describes the data and methods used. The results are presented in Section 3. The study concludes with a summary and discussion in Section 4.

2. Data and Methods

The spaceborne CALIPSO lidar CALIOP (Winker et al., 2009) has collected three-dimensional information on the positions of aerosol and cloud layers during the period from July 2006 to June 2023. The CALIPSO Level-2 Cloud Profile product (05 kmCPro, v4.20, v4.21 from 2020, NASA/LARC/SD/ASDC (2018)) provides a variety of parameters related to clouds with a horizontal resolution of 5 km along the CALIPSO ground track and a vertical resolution of 30 m below 8.2 km height and 60 m between 8.2 and 20.2 km height. The related cloud profiles were found to agree well with cloud observations of the lidar on the International Space Station (Tesche & Noel, 2022). Following Tesche et al. (2021) and Tesche and Noel (2022), we use the Vertical Feature Mask (Liu et al., 2009) to obtain information on the extent and type of tropospheric clouds. The extracted parameters include time, latitude, longitude, the day–night flag, and the number of height bins related to the occurrence of the eight cloud types in the cloud mask: (a) low overcast, transparent; (b) low overcast, opaque; (c) transition stratocumulus; (d) low, broken cumulus; (e) altocumulus (transparent); (f) altostratus (opaque); (g) cirrus (transparent); and (h) deep convective (opaque). The four low-cloud types are defined as having a cloud-top height below 680 hPa and the height of the uppermost cloud bin in any of those types (if available in a profile) is considered as Z_{top} in our analysis. CALIPSO left its orbit within the A-Train in October 2018. From thereon, its overpass time started to drift to about 105 min in 2023 but the lowering of the orbit had no effect on the height of detected features (Chepfer et al., 2025). As a consequence and similar to Liu et al. (2024), we therefore limit our investigation to data until June 2020, when the temporal drift did not yet exceed 30 min and diurnal variation in cloudiness is unlikely to assert an effect on the obtained statistics.

Based on this information, each cloud profile is categorized as cloud-free (no cloud is detected at any height), cloudy (any cloud type is detected at any height), or low-level clouds only (any low cloud type is detected). The

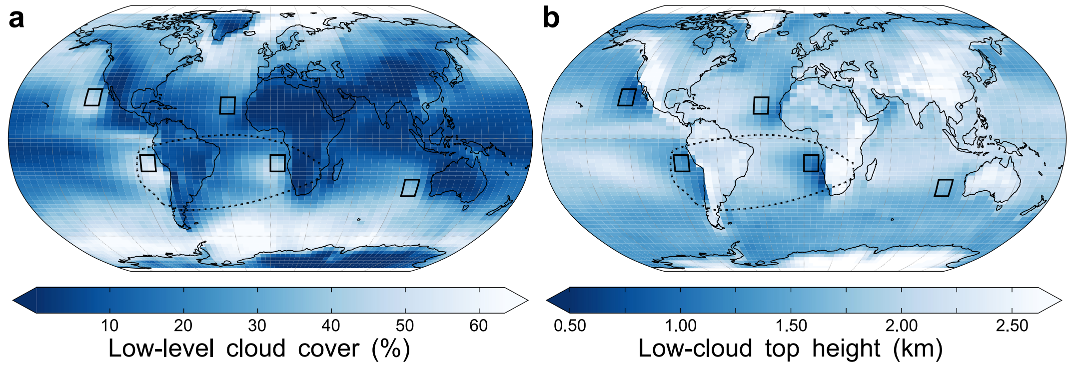

Figure 1. Mean unobscured low-level cloud cover (a) and low-cloud top height (b) above sea level as derived from CALIPSO lidar observations between July 2006 and June 2020. The dotted line marks the SAA. Boxes show the classic stratocumulus regions of Klein and Hartmann (1993).

occurrence of these three categories, as well as the cloud-top height, is then gridded to monthly maps with a resolution of 2.5° longitude by 1.25° latitude. Analogous to Scott et al. (2020) and as recommended in Zelinka et al. (2025), we account for the obscuration of LCC by defining LCC as

$$LCC = \frac{CC_{\mathrm{low}}}{CC_{\mathrm{all\text{-}sky}} - (CC_{\mathrm{cloudy}} - CC_{\mathrm{low}})}. \quad (1)$$

Here, $CC_{\mathrm{all\text{-}sky}}$ refers to the total number of (cloud-free and cloudy) profiles in a grid box, while CC_{cloudy} and CC_{low} separate cloudy and low-level cloud only profiles, respectively. The analysis is performed considering all observations, as well as for data collected only during day and night, respectively.

CALIPSO does not capture the full diurnal cycle of LCC and Z_{top} as its overpasses occur at fixed local times of 0130 and 1330. Lidar measurements based on the International Space Station, whose orbit is not sun-synchronous, indicate that CALIPSO LCC is close to the daily extremes of LCC over ocean (maximum during night, minimum during day) and is more representative of daily averages over land (Noel et al., 2018). In any case, the deviation from the diurnal mean over the ocean is generally below 5% and further minimized in our analysis by averaging observations during day and night.

We use multiple data sets for SST and EIS as cloud-controlling factors. This is because trends in reanalysis data sets can be uncertain, especially in the case of EIS (Ceppi et al., 2026; Zelinka et al., 2026). Specifically, we consider global monthly-mean SST and EIS (Wood & Bretherton, 2006) fields over the CALIOP time period. Data are taken from the European Center for Medium-Range Weather Forecasts (ECMWF) reanalysis, version 5 (ERA5; Copernicus Climate Change Service, 2023a, 2023b; Hersbach et al., 2020), the Atmospheric Infrared Sounder (AIRS) satellite product, version 7 (AIRS project, 2019; Aumann et al., 2003), and the National Oceanic and Atmospheric Administration (NOAA) Optimum Interpolation (OI) SST product, version 2 (Huang et al., 2021; Reynolds et al., 2002). For the AIRS-based EIS, we use the 700-hPa temperature from AIRS in combination with 1000-hPa temperature from ERA5 as in Ceppi et al. (2026). All parameters are re-gridded to match the resolution of the CALIOP data set.

Monthly LCC and Z_{top} over the time period from July 2006 to June 2020 are investigated for linear trends. We estimate the sensitivities of LCC and Z_{top} to SST and EIS by separately regressing local detrended low-cloud anomalies onto local detrended anomalies of SST and EIS. Strictly referring to the low-level clouds within those regions, we aggregate the sensitivities by large-scale climatological cloud regimes of stratocumulus (Sc), trade cumulus (Tc), tropical ascending (Ta), and mid-latitude (Ml) following Scott et al. (2020) and Andersen et al. (2023). Cloud regime regions are defined by threshold values of climatological EIS and vertical velocity at 700 hPa, as summarized in Figure 4a. We extend these cloud regimes by a regime of polar low clouds, defined as occurring at latitudes greater than 67°. For reference to findings in the literature, we furthermore provide sensitivities for the classic stratocumulus regions of Klein and Hartmann (1993), that is, Peruvian, Namibian, Californian, Australian, Canarian stratocumulus.

10.1029/2026GL122478

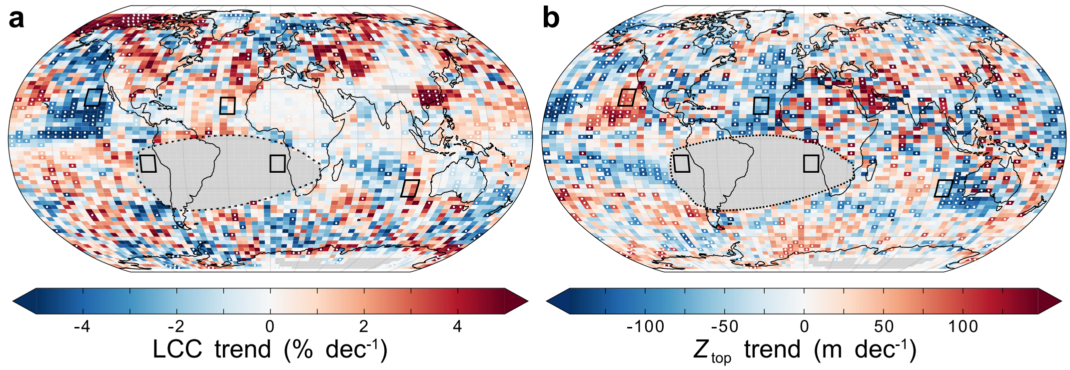

Figure 2. Trends in unobscured low-level cloud cover (a) and low-cloud top height (b) as derived from CALIOP observations between July 2006 and June 2020. Significant trends (p-value <0.05) are highlighted with a marker. Regions with excluded data are marked gray (see Methods section). Lines and boxes as in Figure 1.

From 2016 onward, CALIOP experienced problems with low-energy laser pulses in the region of the South Atlantic Anomaly (SAA, Chepfer et al., 2025; Tackett et al., 2025). This leads to an artificial reduction in general cloudiness and LCC as defined in Equation 1 over the affected region. As a consequence, the region of the SAA is excluded from the trend analysis presented here.

3. Results and Discussion

Figure 1 presents the 14-year means of LCC and Z_{top} from CALIOP observations. Regions of persistent LCC larger than 50% are found over the cold subtropical eastern oceans (Wood, 2012). In addition, similarly large LCC is found over the Arctic Ocean, the Southern Ocean, and the tropical east Pacific around the equator. Note that LCC as defined here is low over the Maritime Continent, as low clouds in this region are frequently obscured by higher-level clouds. This is presented more directly in the geographical distribution of CALIOP profiles that contain only low-level clouds in Figure S1 of Supporting Information S1. The overall distribution of LCC is very similar to the fraction of water clouds in Figure 2d of Seo et al. (2025), which used passive remote sensing. In contrast, the use of the CALIOP observations allows for an unambiguous retrieval of cloud-top height and, thus, cloud cover related to low-level clouds. In fact, the map of mean Z_{top} in Figure 1b illustrates some variation even when considering only low-level clouds, with generally higher elevated cloud tops over land related to orographic features. Over the ocean, we find the characteristic increase in Z_{top} as stratocumulus in shallow boundary layers transition to cumulus in deeper boundary layers further away from the continents (Goren et al., 2025). The climatological patterns of Z_{top} as derived from our CALIOP data set are in good qualitative agreement with known patterns of marine boundary layer height (Possner et al., 2020) and Z_{top} (Zuidema et al., 2009).

The data shown in Figure 1 are used for the trend analysis presented in Figure 2. Note that the trend patterns are somewhat noisy, as expected for a sensor with sparse spatiotemporal sampling (Kotarba, 2022). Nevertheless, the analysis reveals regions with spatially coherent trends. Negative trends in LCC are found over the European Arctic Ocean, the northeast Pacific, and some regions of the Southern Ocean, though the trend is not significant for all grid cells (p-value <0.05). The p-value relates to the trend of the time series from an ordinary least-squares linear regression and is based on a Student's t-test. Positive trends are found over the tropical oceans, some regions of the eastern Pacific, over the southern mid-latitudinal Pacific, the American Arctic Ocean, and eastern China and the South China Sea. Unfortunately, the exclusion of data within the SAA inhibits direct trend estimates for Peruvian and Namibian stratocumulus.

The LCC trend pattern in Figure 2a differs from those obtained from passive remote sensing (Seo et al., 2025) or reanalysis (Goessling et al., 2025) in some regions. Differences can be expected, as different data sets do not represent identical cloud populations, and are influenced by, for example, orbit characteristics, sensor characteristics, and retrieval details (Foster et al., 2023; Marchand, 2013). We find consensus for the decrease in the northeast Pacific (Andersen et al., 2022), and a slight increase in LCC over the tropical south Pacific and around Australia when compared to cloud cover related to water clouds in passive satellite observations (Seo et al., 2025). However, there are large differences over the Southern Ocean, the north Pacific, the Indian Ocean, and the north

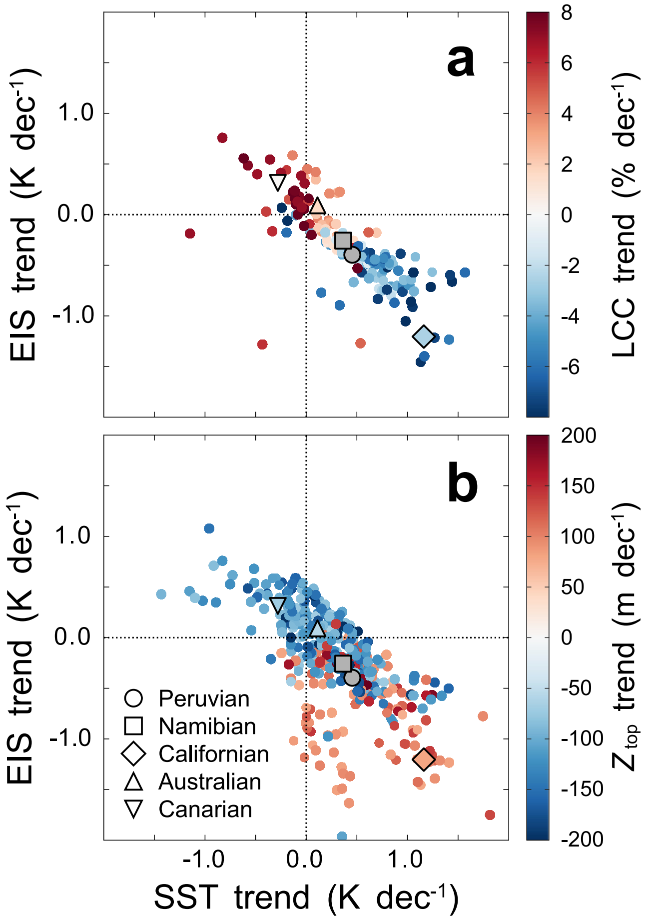

Figure 3. Connection between trends in LCC (top) and Z_{top} (bottom) with respect to EIS and sea-surface temperature (SST) over ocean between July 2006 and June 2020. Points refer to grid boxes that feature significant trends (p-value <0.05) in LCC and Z_{top} with the colors representing the magnitude of that trend. Symbols mark regional mean trends for the stratocumulus boxes shown in Figures 1 and 2. Symbols for Namibian and Peruvian stratocumulus are filled gray due to the absence of reliable CALIPSO observation over the SAA. EIS and SST are based on observations (AIRS and NOAA OI SST).

Atlantic. When compared to ERA5 low cloud cover trends presented in Goessling et al. (2025), our analysis also finds an increase in LCC over the tropical eastern Pacific and a decrease over the north Atlantic (note that their color scale is inverted from ours). However, our data do not reproduce the strong decrease in LCC over the tropical western Pacific and the maritime continent found in the reanalysis data. We attribute this to the fact that those regions feature high upper-level cloud cover that frequently obscure lower-level clouds. Figure S2 in Supporting Information S1 shows the low cloud cover trend in the ERA5 reanalysis for the time period of our CALIOP data set. This analysis illustrates a similar inconsistency in regions of tropical deep convection where the occurrence of unobstructed low clouds is negligible. Consequently, the quantification of low-level cloud trends is less relevant in regions where low-level clouds are frequently obscured by upper-level clouds because they have little direct effect on top-of-atmosphere reflected solar radiation and albedo (Pan et al., 2025). Changes in cloud overlap, or trends in high-cloud occurrence, can therefore influence the radiative balance by exposing trends in low-level clouds (Zelinka et al., 2025).

The trends in Z_{top} in Figure 2b seem to behave exactly opposite to those for LCC, at least for parts of the world such as the Arctic Ocean, the tropical eastern Pacific, and the Southern Ocean. Specifically, there is a widespread decrease in Z_{top} over the north Atlantic and the northeastern Pacific that is consistent with trend patterns derived from passive observations (Seo et al., 2025). The Pearson correlation between global trends in LCC and Z_{top} is −0.22 based on grid cells with significant trends (p-value <0.05) in at least one variable. The correlation increases to −0.56 when repeating the analysis for grid cells in which both variables feature significant trends. Decadal changes in Z_{top} can exceed 100 m. Note that this is more than double the CALIOP height-resolution of 30 m in the altitude range of low-level clouds.

We repeated the analysis shown in Figure 2 separately for daytime and nighttime CALIOP observations (see Figure S3 in Supporting Information S1). While the overall conclusions remain consistent across daytime and nighttime observations, LCC trends over the eastern North Pacific are more pronounced during daytime. This means that earlier dissipation of existing low clouds has to be the cause of the LCC decrease here, rather than a reduction of their nighttime formation. This region includes the Californian stratocumulus deck for which the reduction in LCC during daytime has been found to be caused by the decrease in EIS and the increase by SST—via an increase in the moisture difference between the marine boundary layer and the free troposphere—suggesting cloud dissipation due to dry-air entrainment as the physical mechanism responsible for the LCC decrease (Andersen et al., 2022).

We explore how trends in LCC and Z_{top} over ocean relate to trends in SST and EIS, which are known to exert a strong control over low-level marine clouds (Andersen et al., 2022; Qu et al., 2015). This three-dimensional trend space is presented in Figure 3. We find that trends in SST and EIS are strongly inversely correlated, that is, increasing SST coincides with decreasing EIS and vice versa. This is expected, as near-surface temperature is used for calculating EIS (Wood & Bretherton, 2006). The combination of the two trends furthermore aligns with the observed trends in LCC and Z_{top}. Specifically, regions with the combination of increasing SST and decreasing EIS are associated with decreasing LCC and increasing Z_{top}. In other words, a weaker inversion and a warmer sea surface are clearly connected to a decrease in the occurrence and an increase in the top height of low-level clouds. This co-variability suggests that the anti-correlation between LCC and Z_{top} trends reflects a coherent response of low clouds to changes in large-scale meteorological controls rather than a direct causal relationship between LCC and Z_{top}. In addition to the gridded data, Figure 3 also contains regional averages for five well-studied stratocumulus regions (Klein & Hartmann, 1993). The findings for these regions generally align well with the behavior described above, even though the Canarian region does not show the increase in LCC suggested by the scatter

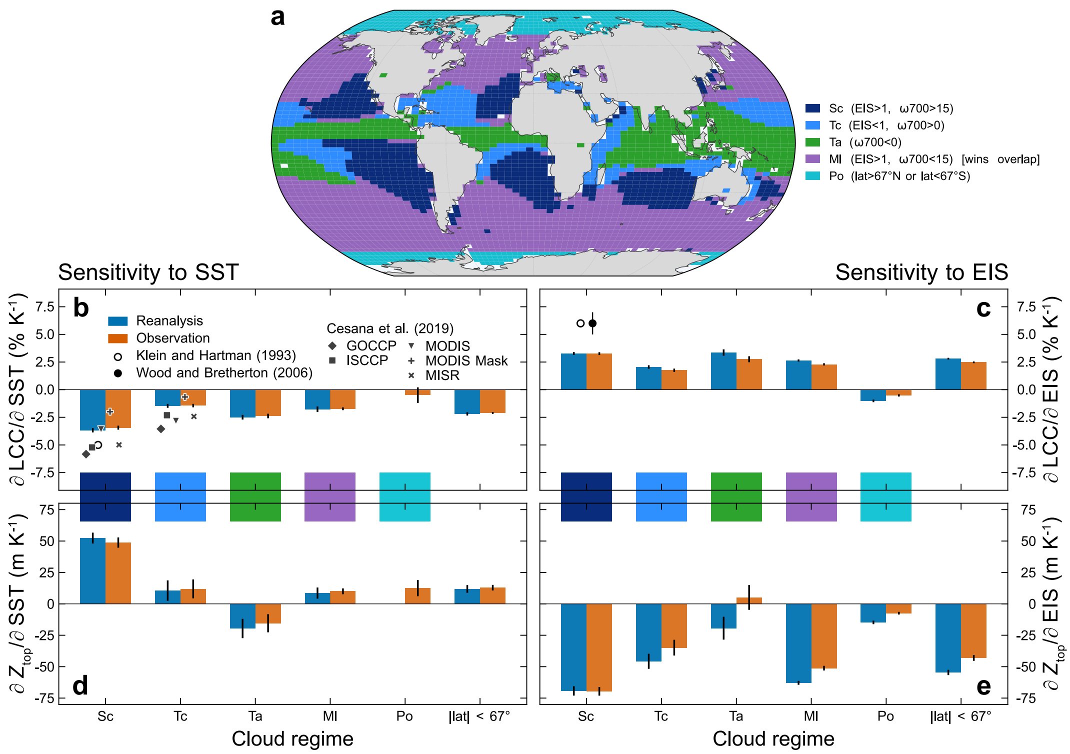

Figure 4. Geographical distribution (a) of stratocumulus (Sc, dark blue), trade cumulus (Tc, light blue), tropical ascending (Ta, green), mid-latitude (Ml, purple), and polar (Po, cyan) cloud regimes. Land areas are marked in gray. Panels (b–e) show mean grid-cell sensitivities with error bars representing the 95 % confidence interval of LCC (top) and Z_{top} (bottom) to sea-surface temperature (left) and EIS (right) based on reanalysis (blue bars) and observational data (orange bars) from July 2006 to June 2020 and separated according to the climatological cloud regimes in (a). The rightmost columns summarize the findings for non-polar clouds. Symbols in (b, c) refer to findings provided in Klein and Hartmann (1993), Wood and Bretherton (2006), and Cesana et al. (2019).

cloud. While we do not have CALIOP-based trends for Namibian and Peruvian stratocumulus, we can expect a decrease in LCC and an increase in Z_{top} from the observed trends in SST and EIS for those regions as well.

Figure 3 is compiled using observational information on SST and EIS and an analysis based on ERA5 (trend maps Figure S4 in Supporting Information S1) gives similar results (not shown). As for the investigation of trends in Figure 2, we have repeated the analysis of Figure 3 for observations during daytime and nighttime. These results are presented in Figure S5 of Supporting Information S1. Daytime observations show little difference compared to Figure 3. However, nighttime observations of LCC show a weaker connection to trends in SST and EIS compared to the daytime observations as discussed above. The trends for Z_{top} are robust independent of the time of observation.

Figure 4; Table S1 in Supporting Information S1 summarize the mean of the local sensitivities of LCC and Z_{top} to SST and EIS and their respective uncertainties for different cloud regimes. The inferred sensitivities are consistent for the observational and reanalysis SST and EIS data sets. A warmer sea surface is associated with a decrease in low-level cloudiness in all climatological cloud regime regions with the largest sensitivity of around -3.8 % K^{-1} for the stratocumulus regions. For comparison, values in the range from -2.0 to -5.8 % K^{-1} are found in Cesana et al. (2019), depending on the considered data set, while Klein and Hartmann (1993) provide a value of -5.0 % K^{-1}. Cesana et al. (2019) provide sensitivities of -0.6 to -3.5 % K^{-1} for trade cumulus compared to our finding of -1.5 % K^{-1}. The observed differences in these comparisons can arise from different sources related to LCC. The sparsity of the CALIOP observations can lead to a representativeness error, introducing small-scale variability in LCC that is statistically independent of large-scale SST/EIS fields. This reduces the signal-to-noise ratio and leads to the attenuation of the estimated sensitivity toward zero. Ambiguities in the LCC derived from passive sensors and not accounting for obscuration by higher-level clouds are further factors that are likely to contribute to differences in estimated LCC sensitivity to SST and EIS. Also, the relatively short time periods of the various satellite records (typically <25 years) are major contributors to uncertainties of sensitivity estimates (Klein et al., 2017). Low-level clouds in the tropical ascending and mid-latitudinal cloud regimes show LCC-SST sensitivities between those for trade cumulus and stratocumulus, and on the order of -2.0 % K^{-1} for non-polar clouds. Polar low-level clouds show an almost negligible sensitivity of LCC to SST. In contrast to SST, we find a more or less similar increase in LCC of around 2.5 % K^{-1} across cloud regimes (except for polar clouds that show a small negative sensitivity) with increasing EIS (Figure 4c). Our estimates for LCC sensitivity to EIS for stratocumulus is smaller than those of about 6.0 % K^{-1} presented in Klein and Hartmann (1993) and Wood and Bretherton (2006).

To our knowledge, this study is the first to report global, regime-resolved estimates of the sensitivity of Z_{top} to SST and EIS as shown in Figures 4d and 4e, respectively. We find that Z_{top} is particularly sensitive to SST for low-level clouds in the stratocumulus regime with around 50 m K^{-1} compared to around 10 m K^{-1} for those in the trade cumulus, mid-latitude, and polar low-level cloud regimes, and between -15 and -20 m K^{-1} for low-level clouds in the tropical ascending regime. This is consistent with other observational studies that find decreasing cloud fraction and increasing Z_{top} with SST in stratocumulus regions (Cesana et al., 2019), but a weaker cloud-fraction response in trade-cumulus regions (Ceppi et al., 2024; Cesana & Del Genio, 2021; Cesana et al., 2019; Myers et al., 2021). Since reproducing the observed vertical structure of the low-cloud response is important for realistic modeling of LCC–SST sensitivities (Cesana et al., 2019), the Z_{top} sensitivities derived here may provide an effective observational constraint on modeled low-level clouds and the boundary-layer response. The pronounced stratocumulus sensitivity to SST is physically consistent with the strong coupling between SST, boundary-layer depth, and cloud regime in subtropical stratocumulus regions. Increased SSTs can enhance surface turbulent fluxes, promote cloud-layer decoupling, and strengthen entrainment of warm and dry free-tropospheric air, thereby favoring a deeper marine boundary layer and a transition from extensive stratocumulus to more broken cumulus with higher cloud-tops (Bretherton & Wyant, 1997; Liu et al., 2024). This regime-transition perspective also helps to explain the negative correlation between LCC and Z_{top} trends: conditions that reduce LCC, such as warmer SST and weaker inversion strength, can simultaneously raise cloud tops by favoring deeper, more weakly capped boundary layers. Conversely, cooler SST or stronger EIS suppress boundary-layer deepening, maintain shallower cloud tops, and favor more extensive stratiform LCC. Changes in low cloud organization (Denby, 2020), as well as alterations in the stratocumulus-to-cumulus transition that coincide with changes in Z_{top} (Choudhury & Goren, 2024; Goren et al., 2025), have been shown to affect both longwave and shortwave radiative effects. This suggests that trends in LCC influence not only shortwave radiation through changes in cloud cover, but also other components of the radiative effect.

The negative sensitivity of Z_{top} to EIS is more pronounced than the positive one related to SST. Large values of around -70 m K^{-1} for Stratocumulus, around -55 m K^{-1} for mid-latitude low-level clouds, and around -40 m K^{-1} for trade cumulus lead to a near-global estimate (excluding the polar regions) of around 50 m K^{-1}.

4. Summary and Conclusions

In contrast to passive remote sensing from space, spaceborne lidar is capable of unambiguously detecting the height at which a cloud layer occurs. We have used this advantage here to investigate potential trends in the occurrence and top height of low-level clouds based on 14 years of CALIPSO lidar observations. Profile-based information on LCC and Z_{top} obtained from the CALIPSO vertical feature mask is aggregated to gridded monthly means which are applied for trend analysis in combination with meteorological data based on observations and ERA5 reanalysis. Specifically, we relate trends in the occurrence and top height of low-level clouds to coinciding trends in surface temperature and atmospheric stability. Because of instrumental constraints (Chepfer et al., 2025), we have to exclude observations within the SAA from the analysis. To our knowledge, this is the first global, regime-resolved quantification of the sensitivity of low-level cloud-top height to SST and EIS using active satellite observations.

Our analysis shows pronounced trends in LCC and Z_{top} over the eastern Pacific and the north Atlantic. Identified trends of LCC and Z_{top} are anti-correlated, and strongly related to trends in surface temperature and EIS, suggesting that both quantities respond coherently to changing large-scale meteorological controls. We find a consistent negative (positive) sensitivity of low clouds in different regimes to changes in SST (EIS) that is in line with earlier work. In contrast to earlier studies, we base our LCC on active remote-sensing observations that are very sensitive to cloud-top height and allow for an unambiguous identification of low-level clouds.

In addition to LCC, we provide a first global, regime-resolved quantification of the sensitivity of Z_{top} to changes in SST and EIS. Cloud-top height sensitivity to SST changes is most pronounced for stratocumulus with an increase of about $50\,\mathrm{m\,K^{-1}}$. This is consistent with warmer SST favoring deeper boundary layers, enhanced entrainment and decoupling, and, in stratocumulus regions, a transition toward cumulus with higher cloud tops (Wyant et al., 1997). Sensitivities are small but positive for low-level clouds in other cloud regimes except for the tropical ascending regime in which a decrease in Z_{top} of about $20\,\mathrm{m\,K^{-1}}$ is found. As one might expect, our analysis shows that cloud-top height decreases with increasing EIS, that is, as the atmosphere becomes more stably stratified. This is particularly pronounced for stratocumulus and mid-latitude low-level clouds for which the sensitivity exceeds $-50\,\mathrm{m\,K^{-1}}$. While the relatively short CALIPSO record, sparse lidar sampling, and necessary exclusion of the SAA limit the robustness of regional trend estimates, the results improve our understanding of low-cloud responses to changing large-scale meteorological conditions and provide a baseline for evaluating and constraining numerical model simulations.

Conflict of Interest

The authors declare no conflicts of interest relevant to this study.

Availability Statement

All data sets used in this work are publicly available. The CALIPSO Level 2 Aerosol Profile product can be accessed at NASA/LARC/SD/ASDC (2018) (last accessed: 26.05.2026). ERA5 reanalysis data are available at Copernicus Climate Change Service (2023a, 2023b) (last accessed: 26.05.2026). The AIRS satellite product, version 7 can be downloaded at AIRS project (2019) (last accessed: 26.05.2026). The NOAA OI SST product, version 2 is described in Reynolds et al. (2002) and Huang et al. (2021) (last accessed: 26.05.2026).

Acknowledgments

This research was supported by the German Research Foundation (Deutsche Forschungsgemeinschaft, DFG; Grants 524386224 and 554554120) and the Israel Science Foundation (Grant 3171/24). Additional support was provided by the Federal State of Saxony and the European Social Fund (ESF) in the framework of the programme "Projects in the fields of higher education and research" (Grant 100649813). HA was supported by the Helmholtz Association through PoF IV in the Research Field Earth and Environment under the programme Changing Earth–Sustaining our Future. Open Access funding enabled and organized by Projekt DEAL.

References

AIRS project. (2019). Aqua/AIRS L3 monthly standard physical retrieval (AIRS-only) 1 degree x 1 degree V7.0 [Dataset]. *Goddard Earth Sciences Data and Information Services Center (GES DISC)*. https://doi.org/10.5067/UBENJB9D3T2H

Andersen, H., Cermak, J., Douglas, A., Myers, T. A., Nowack, P., Stier, P., et al. (2023). Sensitivities of cloud radiative effects to large-scale meteorology and aerosols from global observations. *Atmospheric Chemistry and Physics*, *23*(18), 10775–10794. https://doi.org/10.5194/acp-23-10775-2023

Andersen, H., Cermak, J., Fuchs, J., Knutti, R., & Lohmann, U. (2017). Understanding the drivers of marine liquid-water cloud occurrence and properties with global observations using neural networks. *Atmospheric Chemistry and Physics*, *17*(15), 9535–9546. https://doi.org/10.5194/acp-17-9535-2017

Andersen, H., Cermak, J., Zipfel, L., & Myers, T. A. (2022). Attribution of observed recent decrease in low clouds over the northeastern Pacific to cloud-controlling factors. *Geophysical Research Letters*, *49*(3), 1–10. https://doi.org/10.1029/2021gl096498

Aumann, H., Chahine, M., Gautier, C., Goldberg, M., Kalnay, E., McMillin, L., et al. (2003). AIRS/AMSU/HSB on the Aqua mission: Design, science objectives, data products, and processing systems. *IEEE Transactions on Geoscience and Remote Sensing*, *41*(2), 253–264. https://doi.org/10.1109/TGRS.2002.808356

Bretherton, C. S., & Wyant, M. C. (1997). Moisture transport, lower-tropospheric stability, and decoupling of cloud-topped boundary layers. *Journal of the Atmospheric Sciences*, *54*(1), 148–167. https://doi.org/10.1175/1520-0469(1997)054⟨0148:MTLTSA⟩2.0.CO;2

Cao, Y., Zhu, Y., Wang, M., Rosenfeld, D., Zhou, C., Liu, J., et al. (2024). Improving prediction of marine low clouds using cloud droplet number concentration in a convolutional neural network. *Journal of Geophysical Research: Machine Learning and Computation*, *1*(4), e2024JH000355. https://doi.org/10.1029/2024jh000355

Ceppi, P., Myers, T. A., Nowack, P., Wall, C. J., & Zelinka, M. D. (2024). Implications of a pervasive climate model bias for low-cloud feedback. *Geophysical Research Letters*, *51*(20), e2024GL110525. https://doi.org/10.1029/2024GL110525

Ceppi, P., Wilson Kemsley, S., Andersen, H., Andrews, T., Kramer, R. J., Nowack, P., et al. (2026). Emerging low-cloud feedback and adjustment in global satellite observations. *Atmospheric Chemistry and Physics*, *26*(6), 4153–4171. https://doi.org/10.5194/acp-26-4153-2026

Cesana, G., & Del Genio, A. D. (2021). Observational constraint on cloud feedbacks suggests moderate climate sensitivity. *Nature Climate Change*, *11*(3), 213–218. https://doi.org/10.1038/s41558-020-00970-y

Cesana, G., Del Genio, A. D., Ackerman, A. S., Kelley, M., Elsaesser, G., Fridlind, A. M., et al. (2019). Evaluating models' response of tropical low clouds to SST forcings using CALIPSO observations. *Atmospheric Chemistry and Physics*, *19*(5), 2813–2832. https://doi.org/10.5194/acp-19-2813-2019

Chepfer, H., Chomette, O., Arouf, A., Noel, V., Winker, D., Feofilov, A., & Alava Baldazo, A. (2025). Variability and trends in cloud properties over 17 years from calipso space lidar observations. *Journal of Geophysical Research: Atmospheres*, *130*(20), e2025JD043764. https://doi.org/10.1029/2025JD043764

Choudhury, G., & Goren, T. (2024). Thin clouds control the cloud radiative effect along the sc-cu transition. *Journal of Geophysical Research: Atmospheres*, *129*(10), e2023JD040406. https://doi.org/10.1029/2023JD040406

Christensen, M. W., Jones, W. K., & Stier, P. (2020). Aerosols enhance cloud lifetime and brightness along the stratus-to-cumulus transition. *Proceedings of the National Academy of Sciences*, *117*(30), 17591–17598. https://doi.org/10.1073/pnas.1921231117

Copernicus Climate Change Service, C. D. S. (2023a). ERA5 hourly data on single levels from 1940 to present [Dataset]. *Copernicus Climate Change Service (C3S) Climate Data Store (CDS)*. https://doi.org/10.24381/cds.adbb2d47

Copernicus Climate Change Service, C. D. S. (2023b). ERA5 hourly data on pressure levels from 1940 to present [Dataset]. *Copernicus Climate Change Service (C3S) Climate Data Store (CDS)*. https://doi.org/10.24381/cds.bd0915c6

Denby, L. (2020). Discovering the importance of mesoscale cloud organization through unsupervised classification. *Geophysical Research Letters*, *47*(1), e2019GL085190. https://doi.org/10.1029/2019GL085190

Eastman, R., Warren, S. G., & Hahn, C. J. (2011). Variations in cloud cover and cloud types over the ocean from surface observations, 1954–2008. *Journal of Climate*, *24*(22), 5914–5934. https://doi.org/10.1175/2011JCLI3972.1

Forster, P., Storelvmo, T., Armour, K., Collins, W., Dufresne, J.-L., Frame, D., et al. (Eds.), Climate change 2021: The physical science basis (pp. 923–1054). Cambridge University Press. https://doi.org/10.1017/9781009157896.009

Foster, M. J., Phillips, C., Heidinger, A. K., Borbas, E. E., Li, Y., Menzel, W. P., et al. (2023). PATMOS-x version 6.0: 40 years of merged AVHRR and HIRS global cloud data. *Journal of Climate*, *36*(4), 1143–1160. https://doi.org/10.1175/JCLI-D-22-0147.1

Geiss, A., & Marchand, R. (2019). Cloud responses to climate variability over the extratropical oceans as observed by misr and modis. *Atmospheric Chemistry and Physics*, *19*(11), 7547–7565. https://doi.org/10.5194/acp-19-7547-2019

Goessling, H. F., Rackow, T., & Jung, T. (2025). Recent global temperature surge intensified by record-low planetary albedo. *Science*, *387*(6729), 68–73. https://doi.org/10.1126/science.adq7280

Goode, P. R., Pallé, E., Shoumko, A., Shoumko, S., Montañes-Rodriguez, P., & Koonin, S. E. (2021). Earth's albedo 1998–2017 as measured from earthshine. *Geophysical Research Letters*, *48*(17), e2021GL094888. https://doi.org/10.1029/2021GL094888

Goren, T., Choudhury, G., Kretzschmar, J., & McCoy, I. (2025). Co-variability drives the inverted-v sensitivity between liquid water path and droplet concentrations. *Atmospheric Chemistry and Physics*, *25*(6), 3413–3423. https://doi.org/10.5194/acp-25-3413-2025

Goren, T., Feingold, G., Gryspeerdt, E., Kazil, J., Kretzschmar, J., Jia, H., & Quaas, J. (2022). Projecting stratocumulus transitions on the albedo—cloud fraction relationship reveals linearity of albedo to droplet concentrations. *Geophysical Research Letters*, *49*(20), e2022GL101169. https://doi.org/10.1029/2022GL101169

Hersbach, H., Bell, B., Berrisford, P., Hirahara, S., Horányi, A., Muñoz-Sabater, J., et al. (2020). The ERA5 global reanalysis. *Quarterly Journal of the Royal Meteorological Society*, *146*(730), 1999–2049. https://doi.org/10.1002/qj.3803

Huang, B., Liu, C., Banzon, V., Freeman, E., Graham, G., Hankins, B., et al. (2021). Improvements of the daily optimum interpolation sea surface temperature (doisst) version 2.1. *Journal of Climate*, *34*(8), 2923–2939. https://doi.org/10.1175/JCLI-D-20-0166.1

Huo, J., Lu, D., Duan, S., Bi, Y., & Liu, B. (2020). Comparison of the cloud top heights retrieved from modis and ahi satellite data with ground-based ka-band radar. *Atmospheric Measurement Techniques*, *13*(1), 1–11. https://doi.org/10.5194/amt-13-1-2020

Jia, Y., Andersen, H., & Cermak, J. (2024). Analysis of the cloud fraction adjustment to aerosols and its dependence on meteorological controls using explainable machine learning. *Atmospheric Chemistry and Physics*, *24*(22), 13025–13045. https://doi.org/10.5194/acp-24-13025-2024

Klein, S. A., Hall, A., Norris, J. R., & Pincus, R. (2017). Low-Cloud feedbacks from cloud-controlling factors: A review. *Surveys in Geophysics*, *38*(6), 1307–1329. https://doi.org/10.1007/s10712-017-9433-3

Klein, S. A., & Hartmann, D. L. (1993). The seasonal cycle of low stratiform clouds. *Journal of Climate*, *6*(8), 1587–1606. https://doi.org/10.1175/1520-0442(1993)006⟨1587:TSCOLS⟩2.0.CO;2

Kotarba, A. Z. (2022). Impact of the revisit frequency on cloud climatology for CALIPSO, EarthCARE, Aeolus, and ICESat-2 satellite lidar missions. *Atmospheric Measurement Techniques*, *15*(14), 4307–4322. https://doi.org/10.5194/amt-15-4307-2022

Liu, J.-W., Yang, L., & Xie, S.-P. (2024). CALIPSO observed low clouds over the subtropical Northeast Pacific: Summer climatology and interannual variability. *Journal of Geophysical Research: Atmospheres*, *129*(8), e2023JD039168. https://doi.org/10.1029/2023JD039168

Liu, Z., Vaughan, M., Winker, D., Kittaka, C., Getzewich, B., Kuehn, R., et al. (2009). The CALIPSO lidar cloud and aerosol discrimination: Version 2 algorithm and initial assessment of performance. *Journal of Atmospheric and Oceanic Technology*, *26*(7), 1198–1213. https://doi.org/10.1175/2009JTECHA1229.1

Loeb, N. G., Thorsen, T. J., Norris, J. R., Wang, H., & Su, W. (2018). Changes in earth's energy budget during and after the "pause" in global warming: An observational perspective. *Climate*, *6*(3), 62. https://doi.org/10.3390/cli6030062

Marchand, R. (2013). Trends in ISCCP, MISR, and MODIS cloud-top-height and optical-depth histograms. *Journal of Geophysical Research: Atmospheres*, *118*(4), 1941–1949. https://doi.org/10.1002/jgrd.50207

Mauritsen, T., Tsushima, Y., Meyssignac, B., Loeb, N. G., Hakuba, M., Pilewskie, P., et al. (2025). Earth's energy imbalance more than doubled in recent decades. *AGU Advances*, *6*(3), e2024AV001636. https://doi.org/10.1029/2024AV001636

McCoy, D. T., Eastman, R., Hartmann, D. L., & Wood, R. (2017). The change in low cloud cover in a warmed climate inferred from AIRS, MODIS, and ERA-interim. *Journal of Climate*, *30*(10), 3609–3620. https://doi.org/10.1175/JCLI-D-15-0734.1

Mitra, A., Di Girolamo, L., Hong, Y., Zhan, Y., & Mueller, K. J. (2021). Assessment and error analysis of terra-modis and misr cloud-top heights through comparison with iss-cats lidar. *Journal of Geophysical Research: Atmospheres*, *126*(9), e2020JD034281. https://doi.org/10.1029/2020JD034281

Myers, T. A., & Norris, J. R. (2016). Reducing the uncertainty in subtropical cloud feedback. *Geophysical Research Letters*, *43*(5), 2144–2148. https://doi.org/10.1002/2015GL067416

Myers, T. A., Scott, R. C., Zelinka, M. D., Klein, S. A., Norris, J. R., & Caldwell, P. M. (2021). Observational constraints on low cloud feedback reduce uncertainty of climate sensitivity. *Nature Climate Change*, *11*(6), 501–507. https://doi.org/10.1038/s41558-021-01039-0

NASA/LARC/SD/ASDC. (2018). CALIPSO lidar level 2 aerosol profile, V4-20 [Dataset]. *NASA*. https://doi.org/10.5067/CALIOP/CALIPSO/LID_L2_05KMAPRO-STANDARD-V4-20

Naud, C. M., Elsaesser, G. S., & Booth, J. F. (2023). Dominant cloud controlling factors for low-level cloud fraction: Subtropical versus extratropical oceans. *Geophysical Research Letters*, *50*(19), e2023GL104496. https://doi.org/10.1029/2023GL104496

Noel, V., Chepfer, H., Chiriaco, M., & Yorks, J. (2018). The diurnal cycle of cloud profiles over land and ocean between 51°S and 51°N, seen by the cats spaceborne lidar from the international space station. *Atmospheric Chemistry and Physics*, *18*(13), 9457–9473. https://doi.org/10.5194/acp-18-9457-2018

Pan, Z., Rosenfeld, D., Zang, L., Yin, J., & Mao, F. (2025). Large warming of tropical convective anvils masked by their underlying clouds. *Remote Sensing of Environment*, *317*, 114524. https://doi.org/10.1016/j.rse.2024.114524

Possner, A., Eastman, R., Bender, F., & Glassmeier, F. (2020). Deconvolution of boundary layer depth and aerosol constraints on cloud water path in subtropical stratocumulus decks. *Atmospheric Chemistry and Physics*, *20*(6), 3609–3621. https://doi.org/10.5194/acp-20-3609-2020

Qu, X., Hall, A., Klein, S. A., & DeAngelis, A. M. (2015). Positive tropical marine low-cloud cover feedback inferred from cloud-controlling factors. *Geophysical Research Letters*, *42*(18), 7767–7775. https://doi.org/10.1002/2015GL065627

Reynolds, R. W., Rayner, N. A., Smith, T. M., Stokes, D. C., & Wang, W. (2002). An improved in situ and satellite SST analysis for climate. *Journal of Climate*, *15*(13), 1609–1625. https://doi.org/10.1175/1520-0442(2002)015⟨1609:AIISAS⟩2.0.CO;2

Scott, R. C., Myers, T. A., Norris, J. R., Zelinka, M. D., Klein, S. A., Sun, M., & Doelling, D. R. (2020). Observed sensitivity of low-cloud radiative effects to meteorological perturbations over the global oceans. *Journal of Climate*, *33*(18), 7717–7734. https://doi.org/10.1175/JCLI-D-19-1028.1

Seo, J., Phillips, C., Heidinger, A. K., & Foster, M. J. (2025). Cloud changes over the tropical and midlatitude ocean over the last four decades using patmos-x version 6.0. *Journal of Climate*, *38*(17), 4351–4368. https://doi.org/10.1175/JCLI-D-24-0581.1

Slingo, A. (1990). Sensitivity of the earth's radiation budget to changes in low clouds. *Nature*, *343*(6253), 49–51. https://doi.org/10.1038/343049a0

Tackett, J. L., Ryan, R. A., Garnier, A. E., Kar, J., Getzewich, B. J., Cai, X., et al. (2025). Mitigating impacts of low energy laser pulses on caliop data products. *Atmospheric Measurement Techniques*, *18*(21), 6211–6231. https://doi.org/10.5194/amt-18-6211-2025

Tesche, M., Achtert, P., & Pitts, M. C. (2021). On the best locations for ground-based polar stratospheric cloud (PSC) observations. *Atmospheric Chemistry and Physics*, *21*(1), 505–516. https://doi.org/10.5194/acp-21-505-2021

Tesche, M., & Noel, V. (2022). Locations for the best lidar view of mid-level and high clouds. *Atmospheric Measurement Techniques*, *15*(14), 4225–4240. https://doi.org/10.5194/amt-15-4225-2022

Winker, D. M., Vaughan, M. A., Omar, A., Hu, Y., Powell, K. A., Liu, Z., et al. (2009). Overview of the CALIPSO mission and CALIOP data processing algorithms. *Journal of Atmospheric and Oceanic Technology*, *26*(11), 2310–2323. https://doi.org/10.1175/2009JTECHA1281.1

Wood, R. (2012). Stratocumulus clouds. *Monthly Weather Review*, *140*(8), 2373–2423. https://doi.org/10.1175/MWR-D-11-00121.1

Wood, R., & Bretherton, C. S. (2006). On the relationship between stratiform low cloud cover and lower-tropospheric stability. *Journal of Climate*, *19*(24), 6425–6432. https://doi.org/10.1175/JCLI3988.1

Wyant, M. C., Bretherton, C. S., Rand, H. a., & Stevens, D. E. (1997). Numerical simulations and a conceptual model of the stratocumulus to trade cumulus transition. *Journal of the Atmospheric Sciences*, *54*(1), 168–192. https://doi.org/10.1175/1520-0469(1997)054⟨0168:NSAACM⟩2.0.CO;2

Zelinka, M. D., Chao, L.-W., Myers, T. A., Qin, Y., & Klein, S. A. (2025). Technical note: Recommendations for diagnosing cloud feedbacks and rapid cloud adjustments using cloud radiative kernels. *Atmospheric Chemistry and Physics*, *25*(3), 1477–1495. https://doi.org/10.5194/acp-25-1477-2025

Zelinka, M. D., Myers, T. A., McCoy, D. T., Po-Chedley, S., Caldwell, P. M., Ceppi, P., et al. (2020). Causes of higher climate sensitivity in CMIP6 models. *Geophysical Research Letters*, *47*(1), e2019GL085782. https://doi.org/10.1029/2019GL085782

Zelinka, M. D., Myers, T. A., Qin, Y., Chao, L.-W., Klein, S. A., Po-Chedley, S., et al. (2026). Recent cloud trends and extremes reaffirm established bounds on cloud feedback and aerosol-cloud interactions. *Communications Earth & Environment*. https://doi.org/10.1038/s43247-026-03461-8

Zuidema, P., Painemal, D., de Szoeke, S., & Fairall, C. (2009). Stratocumulus cloud-top height estimates and their climatic implications. *Journal of Climate*, *22*(17), 4652–4666. https://doi.org/10.1175/2009JCLI2708.1